Naval Research Laboratory

Numerical Simulation of Liquid Slosh in Microgravity

Scott F. Bradford

Image Science and Applications Branch
Remote Sensing Division

June 30, 1999

REPORT DOCUMENTATION PAGE

Form Approved
OMB No. 0704-0188

Public reporting burden for this collection of information is estimated to average 1 hour per response, including the time for reviewing instructions, searching existing data sources, gathering and maintaining the data needed, and completing and reviewing the collection of information. Send comments regarding this burden estimate or any other aspect of this collection of information, including suggestions for reducing this burden, to Washington Headquarters Services, Directorate for Information Operations and Reports, 1215 Jefferson Davis Highway, Suite 1204, Arlington, VA 22202-4302, and to the Office of Management and Budget, Paperwork Reduction Project (0704-0188), Washington, DC 20503.

1. AGENCY USE ONLY (Leave Blank)	2. REPORT DATE June 30, 1999	3. REPORT TYPE AND DATES COVERED Final	
4. TITLE AND SUBTITLE Numerical Simulation of Liquid Slosh in Microgravity			**5. FUNDING NUMBERS** 72-5755-08
6. AUTHOR(S) Scott F. Bradford			
7. PERFORMING ORGANIZATION NAME(S) AND ADDRESS(ES) Naval Research Laboratory Washington, DC 20375-5320			**8. PERFORMING ORGANIZATION REPORT NUMBER** NRL/MR/7260--99-8387
9. SPONSORING/MONITORING AGENCY NAME(S) AND ADDRESS(ES) Office of Naval Research 800 North Quincy Street Arlington, VA 22217-5660			**10. SPONSORING/MONITORING AGENCY REPORT NUMBER**
11. SUPPLEMENTARY NOTES			
12a. DISTRIBUTION/AVAILABILITY STATEMENT Approved for public release; distribution is unlimited.			**12b. DISTRIBUTION CODE**

13. ABSTRACT (Maximum 200 words)

Hyperspectral imaging cameras require smooth motion in order to acquire uncorrupted images. Typically, a camera is mounted on a satellite that then rotates to allow the camera to scan the earth's surface. The rotation of the satellite causes propellant sloshing in its fuel tank, which can disrupt the motion of the satellite and therefore degrade the quality of the hyperspectral images.

The severity of the liquid sloshing has been investigated with a numerical fluid dynamics model called Flow-3D (Flow Science, 1997). This model is well suited for such a problem and has been previously verified by comparing numerical predictions with experimental slosh data in reduced gravity environments (Sicilian and Tegart, 1989, Fisher et al., 1992). The experimental data were collected from drop tower tests, which produce a controlled acceleration environment.

14. SUBJECT TERMS Sloshing Hyperspectral imaging Microgravity Reduced gravity			15. NUMBER OF PAGES 17
			16. PRICE CODE
17. SECURITY CLASSIFICATION OF REPORT UNCLASSIFIED	18. SECURITY CLASSIFICATION OF THIS PAGE UNCLASSIFIED	19. SECURITY CLASSIFICATION OF ABSTRACT UNCLASSIFIED	20. LIMITATION OF ABSTRACT UL

NUMERICAL SIMULATION OF LIQUID SLOSH IN MICROGRAVITY

INTRODUCTION

Hyperspectral imaging cameras require smooth motion in order to acquire uncorrupted images. Typically, a camera is mounted on a satellite that then rotates to allow the camera to scan the earth's surface. The rotation of the satellite causes propellant sloshing in its fuel tank, which can disrupt the motion of the satellite and therefore degrade the quality of the hyperspectral images.

The severity of the liquid sloshing has been investigated with a numerical fluid dynamics model called Flow-3D (Flow Science, 1997). This model is well suited for such a problem and has been previously verified by comparing numerical predictions with experimental slosh data in reduced gravity environments (Sicilian and Tegart, 1989, Fisher et al., 1992). The experimental data were collected from drop tower tests, which produce a controlled acceleration environment.

PROBLEM DESCRIPTION

In the numerical simulations, the satellite's fuel tank was the domain of interest. The simulations began with an initial liquid configuration and the tank was then accelerated in a prescribed manner corresponding to a typical satellite rotating motion. The sloshing fluid exerts forces on the tank, which can be computed by the numerical model and assessed for their impact on the satellite's motion.

Two different masses of liquid have been considered in order to investigate the influence of fuel volume on the resulting forces acting on the tank. The first case is a high mass case with 59.5 kg of propellant, which corresponds to a liquid volume of 0.0593 m^3. The remaining volume of the tank is filled with gas at a pressure equal to 1.29 MPa. Fig. 1 shows three slices of the geometry of the tank along with the initial fluid configuration. Note that z denotes the vertical direction, x and y denote the two lateral directions, and the origin is at the satellite's center of mass. The red area represents the propellant, while the blue area is gas. The tank is spherical in shape with a diameter equal to 0.5588 m and there is a cylindrical sump at the bottom with a diameter of 0.2032 m and height of 0.127 m. There are also two sets of vanes, which are perpendicular to each other, running vertically around the circumference of the tank. The vanes are approximately 0.01905 m high. The second case is a low mass case with 30 kg of fuel, which corresponds to a volume of 0.0299 m^3 and the gas pressure is 783 kPa. This case is illustrated in Fig. 2.

In a low gravity environment, surface tension is the dominant restoring force acting on the liquid-gas interface. This is expressed in terms of the Bond number, which is the ratio of the gravity to surface tension forces and is written as

$$Bo = \frac{\rho g R^2}{\sigma} \qquad (1)$$

where ρ is the liquid density, g is the gravitational acceleration, R is the radius of the tank, and σ is the surface tension coefficient. The liquid is modeled as anhydrous hydrazine and has a density, $\rho=1004.0$ kg/m³ and dynamic viscosity, $\mu = 0.0009$ kg/m s at 25 degrees C, while $\sigma=0.006667$ kg/s². In addition, the wall contact angle is 40 degrees. In the present simulations, $g=0$ was specified and therefore $Bo=0$, which indicates the dominant role of surface tension. Therefore, surface tension was included in the numerical simulations.

The Reynolds number is another important parameter in fluid dynamics. It is the ratio of inertia to viscous forces and can be written as

$$Re = \frac{uL}{v} \qquad (2)$$

where u is a typical liquid velocity, L is a length scale of the flow, and $v=\mu/\rho$ is the kinematic viscosity of the liquid. The Reynolds number also indicates the importance of turbulence. A flow with a larger Re is more turbulent than a similar flow with a smaller Re. The numerical simulations revealed that typical fluid velocities were on the order of 0.005 m/s, while a typical length scale, taken as the depth of flow in the tank, was approximately 0.3 m. This yields an Re of about 1500, which indicates that the flow is laminar. Therefore, turbulence was not considered in the simulations.

THE GOVERNING EQUATIONS

The liquid motion is modeled with the conservation of momentum equations in three orthogonal directions. In addition, the liquid is assumed to be incompressible, and therefore its density remains constant. Also, as previously discussed, the flow is assumed to be laminar. Under these assumptions, the momentum conservation laws reduce to the so-called Navier-Stokes equations, which are written as

$$\frac{\partial u}{\partial t} + u\frac{\partial u}{\partial x} + v\frac{\partial u}{\partial y} + w\frac{\partial u}{\partial z} = \frac{-1}{\rho}\frac{\partial p}{\partial x} + v\left(\frac{\partial^2 u}{\partial x^2} + \frac{\partial^2 u}{\partial y^2} + \frac{\partial^2 u}{\partial z^2}\right) + a_x \qquad (3)$$

$$\frac{\partial v}{\partial t} + u\frac{\partial v}{\partial x} + v\frac{\partial v}{\partial y} + w\frac{\partial v}{\partial z} = \frac{-1}{\rho}\frac{\partial p}{\partial y} + v\left(\frac{\partial^2 v}{\partial x^2} + \frac{\partial^2 v}{\partial y^2} + \frac{\partial^2 v}{\partial z^2}\right) + a_y \qquad (4)$$

$$\frac{\partial w}{\partial t} + u\frac{\partial w}{\partial x} + v\frac{\partial w}{\partial y} + w\frac{\partial w}{\partial z} = \frac{-1}{\rho}\frac{\partial p}{\partial z} + v\left(\frac{\partial^2 w}{\partial x^2} + \frac{\partial^2 w}{\partial y^2} + \frac{\partial^2 w}{\partial z^2}\right) + a_z \qquad (5)$$

where u, v, and w are the velocities in the x, y, and z directions, respectively, while p represents the pressure. Note that the equations are written in terms of a coordinate

system that moves with the tank. The terms a_x, a_y, and a_z denote the components of the acceleration of the tank reference frame with respect to an inertial reference frame. If the moving reference frame undergoes angular accelerations about its origin only, the acceleration terms become

$$a_x = -\left\{\dot{\omega}_y z - \dot{\omega}_z y + 2(\omega_y w - \omega_z v) + \omega_y(\omega_x y - \omega_y x) - \omega_z(\omega_z x - \omega_x z)\right\} \qquad (6)$$

$$a_y = -\left\{\dot{\omega}_z x - \dot{\omega}_x z + 2(\omega_z u - \omega_x w) + \omega_z(\omega_y z - \omega_z y) - \omega_x(\omega_x y - \omega_y x)\right\} \qquad (7)$$

$$a_z = -\left\{\dot{\omega}_x y - \dot{\omega}_y x + 2(\omega_x v - \omega_y u) + \omega_x(\omega_z x - \omega_x z) - \omega_y(\omega_y z - \omega_z y)\right\} \qquad (8)$$

where ω denotes the angular velocity and the dot denotes the angular acceleration. In the present simulations, only the angular velocity and acceleration about the y axis are nonzero. The specific form of ω_y is shown in Fig. 3, while the angular acceleration is calculated by numerically differentiating the angular velocity with respect to time.

The conservation of liquid mass, under the incompressible flow assumption, yields the additional constraint,

$$\frac{\partial u}{\partial x} + \frac{\partial v}{\partial y} + \frac{\partial w}{\partial z} = 0 \qquad (9)$$

Eqs. (3) through (5) and Eq. (9) form a coupled set of nonlinear partial differential equations to be solved for the unknowns u, v, w, and p as functions of space and time. The resulting shear stresses and pressure can then be integrated over the wall of the tank in order to estimate the resulting net forces and moments induced by the sloshing fuel.

The movement of the liquid-gas interface is tracked using an Eulerian approach by measuring fluid movement in and out of the stationary computational cells. This method was first developed by Hirt and Nichols (1979) and is known as the Volume of Fluid (VOF) method. The fluid movement is tracked by solving the following transport equation,

$$\frac{\partial F}{\partial t} + u\frac{\partial F}{\partial x} + v\frac{\partial F}{\partial y} + w\frac{\partial F}{\partial z} = 0 \qquad (10)$$

where F is the ratio of the liquid volume in a given cell to the total volume of that cell. This approach can model discontinuous interfaces as well as liquid detachment, which can be extremely important in the simulation of sloshing fluids. Note that this approach neglects the motion of the gas and therefore implicitly assumes that the gas motion has a negligible effect on the movement of the fuel. Also, the gas pressure is assumed to remain constant during the simulation.

NUMERICAL SOLUTION

The governing equations cannot be analytically solved for a complex problem involving sloshing fluids. Therefore, the equations must be solved numerically. As previously mentioned, the numerical model employed in this study is commercially available and is called Flow-3D. It is a finite-difference model that is based on the Marker-And-Cell method developed by Harlow and Welch (1965). All temporal and spatial derivatives in Eqs. (3) through (5), Eq. (9), and Eq. (10) are replaced with finite difference approximations in order to obtain a discrete solution. The model uses a stationary, Cartesian computational grid that may be selectively refined in desired areas. The fuel tank geometry is incorporated into the computational domain by linearly blocking out portions of cells that fall outside of the walls of the tank. Corresponding values of cell volumes and faces that are open to flow are then computed and used in the discrete equations to compute the spatial gradients of velocity, pressure, and F (Hirt and Sicilian, 1985). The grid is staggered, with p and F defined at cell centers, while the velocities are defined at cell faces, as shown in Fig. 4. This prevents "checkerboard" solutions that can result in incompressible flow computations when the velocity and pressure become unlinked at adjacent computational nodes (Patankar, 1980).

The model solves the momentum and incompressibility equations in an iterative manner using a pressure correction scheme. A computationally efficient scheme may be obtained by differentiating Eqs. (3) through (5) in space and substituting the results into Eq. (9). This yields a Poisson equation for p at the new time level $n+1$. This equation is solved by Successive Overrelaxation (SOR) and the new pressure is then used to compute new velocity estimates by solving the discrete analogs of Eqs. (3) through (5). The new velocity estimates are then used to compute a new pressure field via the Poisson equation and this process is continued until the change in p becomes smaller than some tolerance. At this point, the new flow field is known and is then used to compute the new free surface configuration by solving the discrete version of Eq. (10). Boundary conditions are then applied to all flow parameters, which completes the solution for one time step.

Boundary conditions are applied as follows. At the walls of the tank, the velocity perpendicular to the wall is set to zero. Velocities tangent to the wall are set according to the local wall shear stress, which depends on the local Re. At the liquid-gas interface, velocities outside the liquid are extrapolated from the interior such that the resulting tangential shear stress is zero. The pressure in a cell containing a liquid-gas interface is extrapolated from the interface. Surface tension is converted to an equivalent pressure that is specified at the liquid-gas interface. When a solid wall is in contact with a liquid-gas interface, the wall adhesion force is also estimated using the specified wall contact angle. The net force is then converted to an equivalent interface pressure.

The domain was divided into 125,000 equal-sized, cube-shaped cells. The grid spacing in the x direction, Δx, was 0.011 m. The grid spacings in the other directions, Δy and Δz, were the same. The time increment, Δt, varied during the computation and was automatically chosen by the model to maintain the stability and accuracy of the solution.

Additional simulations were performed with 216,000 cells in order to check the convergence of the model. Also, more accurate discrete approximations to the spatial and temporal derivatives were employed as an additional test. Neither refinement led to significant changes in the numerical solutions.

MODEL RESULTS

Fig. 5 shows plots of the pressure contours and velocity vectors for the high fuel mass case. The plots are for the x-z plane at y=0. The first frame shows the flow field at t=40 s. At this point, the tank has just finished moving upward and has just begun its descent. It is seen that the fuel is continuing to move in a counterclockwise direction due to inertia and much of the fuel has moved away from the top of the tank down toward the sump. The next frame is at t=96 s, at which time the tank has just finished accelerating downward, but continues downward at a constant angular velocity. The fuel has been dragged by the tank walls into a clockwise motion, and fuel has moved back toward the right side of the tank. At t=228 s, the downward movement has been completed and the tank is accelerating upward again. Again, the fuel motion is still clockwise due to inertia. At t=280 s, the tank has completed its upward motion and is beginning to descend again. A strong counterclockwise flow induced by the tank motion is clearly evident in the figure. At t=320 s, the tank has completed its downward motion and has come to rest. However, the strong counterclockwise current has only been damped by the downward movement of the tank. At t=400s, there is still significant fuel motion. Slowly, viscous damping would dissipate the remaining kinetic energy of the liquid and surface tension would restore the liquid-gas interface to its equilibrium configuration.

Fig. 6 shows plots of the pressure contours and velocity vectors for the low fuel mass case. These plots are for the same plane as the previous case. The fuel behaves in much the same manner as in the previous case. However, the smaller fuel volume allows some areas of the wall of the tank to become dry.

Fig. 7 compares the forces acting on the fuel tank in the x, y, and z directions for the two cases. F_x denotes the force in the x direction, while F_y and F_z denote the forces acting in the y and z directions, respectively. As expected, F_x and F_y are quite small and have no discernable harmonic components since most of the fluid motion was in the z direction. F_z is slightly larger in magnitude and there is also a more distinct harmonic nature to the force, which is attributable to the satellite's motion. There is no fundamental frequency since the only restoring force in this environment, surface tension, is quite small. Fig. 8 shows the moments about the origin in the x, y, and z directions. M_x and M_z are somewhat smaller than M_y, which is again expected because the tank was rotated about the y axis.

SUMMARY AND CONCLUSIONS

A computational fluid dynamics model has been used to simulate the sloshing of propellant in a satellite fuel tank in a microgravity environment. The resulting forces acting on the tank were computed in order to evaluate their impact on the motion of the satellite. The sloshing was created by a rotating motion, which was chosen to simulate

the scanning motion of the satellite needed for collecting hyperspectral images. A commercial code called Flow-3D was utilized to perform the simulations. The code has been previously verified for sloshing liquid problems in reduced gravity environments and therefore no verification was performed in this study. However, numerical experiments with additional grid refinement and more accurate discrete approximations of the derivatives were performed to verify that the solutions presented here were converged.

In general, the resulting forces and moments acting on the tank were quite small and should have no adverse impact on the motion of the satellite. The harmonic nature of F_z and M_y was due to the satellite motion, and not the restoring force of surface tension. In addition, the amount of fuel in the tank had little impact on the magnitudes of the forces and moments. These results are expected due to the rather gentle motion of the fuel tank.

REFERENCES

Fisher, M.F., Schmidt, G.R., and Martin, J.J. (1992), ``Analysis of Cryogenic Propellant Behaviour in Microgravity and Low Thrust Environments," Cryogenics, Vol. 32, No. 2, pp. 230-235.

Flow Science (1997), *Flow-3D User's Manual*, Flow Science Inc.

Harlow, F.H. and Welch, J.E. (1965), ``Numerical Calculation of Time-Dependent Viscous Incompressible Flow of Fluid With Free Surface, "The Physics of Fluids, Vol. 8, pp. 2182-2189.

Hirt, C.W. and Nichols, B.D., (1981), ``Volume of Fluid (VOF) Method for the Dynamics of Free Boundaries, " Journal of Computational Physics, Vol. 39, pp. 201-225.

Hirt, C.W. and Sicilian, J.M., (1985), ``A Porosity Technique for the Definition of Obstacles in Rectangular Cell Meshes, "Proceedings of the Fourth International Conference on Ship Hydrodynamics, National Academy of Science, Washington D.C.

Sicilian, J.M., and Tegart, J.R. (1989), ``Comparison of Flow-3D Calculations With Very Large Amplitude Slosh Data," The American Society of Mechanical Engineers-Computational Experiments, Vol. 176, Book No. H00491-1989, pp. 23-30.

APPENDIX

The previous simulations were performed in an environment with no gravity acting on the tank or liquid. Therefore, surface tension was the dominant force that acted to restore the system to equilibrium conditions. Since this force is quite weak, no dominant harmonic character was observed in the slosh forces acting on the tank. In order to better demonstrate this, three additional simulations were performed for the same tank

undergoing a constant acceleration in the vertical (z) direction. Three different accelerations equal to $0.00068g$, g, and $3g$ were utilized. The tank was then impulsively perturbed in the x direction and the resulting slosh forces were computed. The power spectral densities (PSD) of the x component of the slosh force are plotted in Fig 9. As a function of frequency. This figure shows that the low acceleration case has a peak in the PSD at a lower frequency than the g acceleration case. Likewise, the g case has its peak PSD value at a lower frequency than the $3g$ case. This is because the larger acceleration creates a more dominant restoring force, which acts more rapidly in bringing the system to equilibrium. This in turn leads to more rapid fuel slosh and therefore a higher frequency in the peak of the PSD.
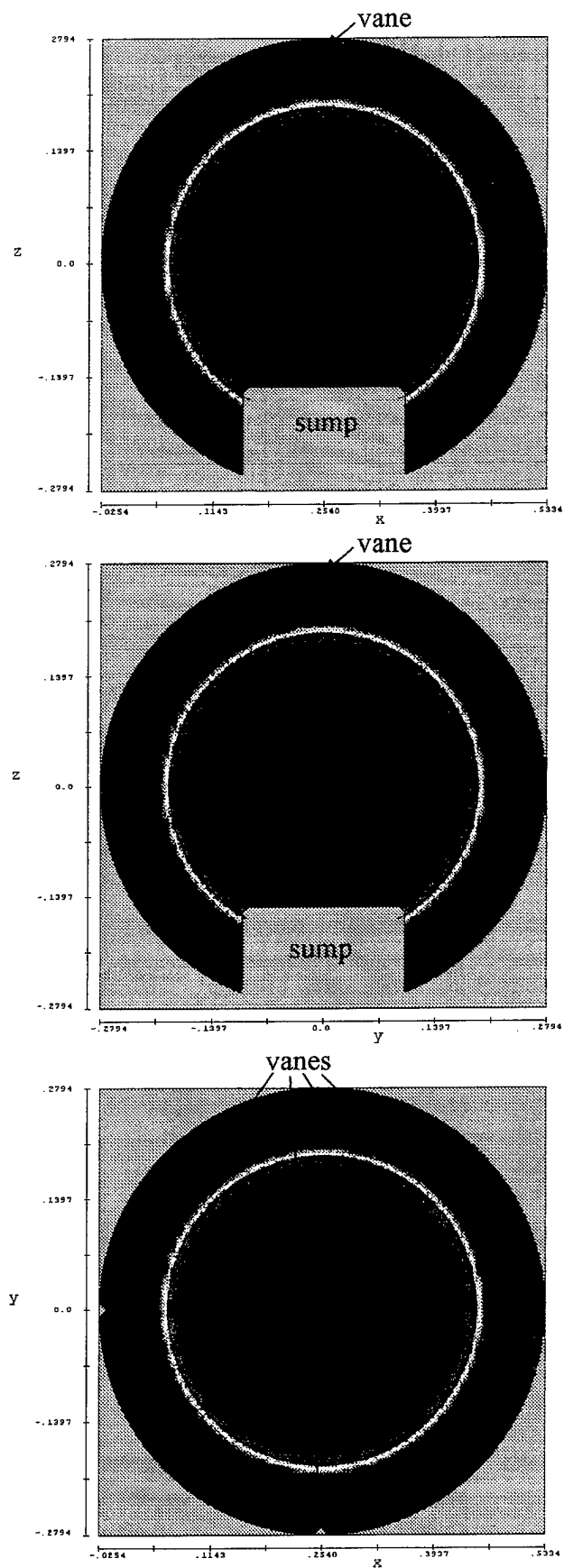
Figure 1: Initial fuel configuration for the high mass case (units in meters).
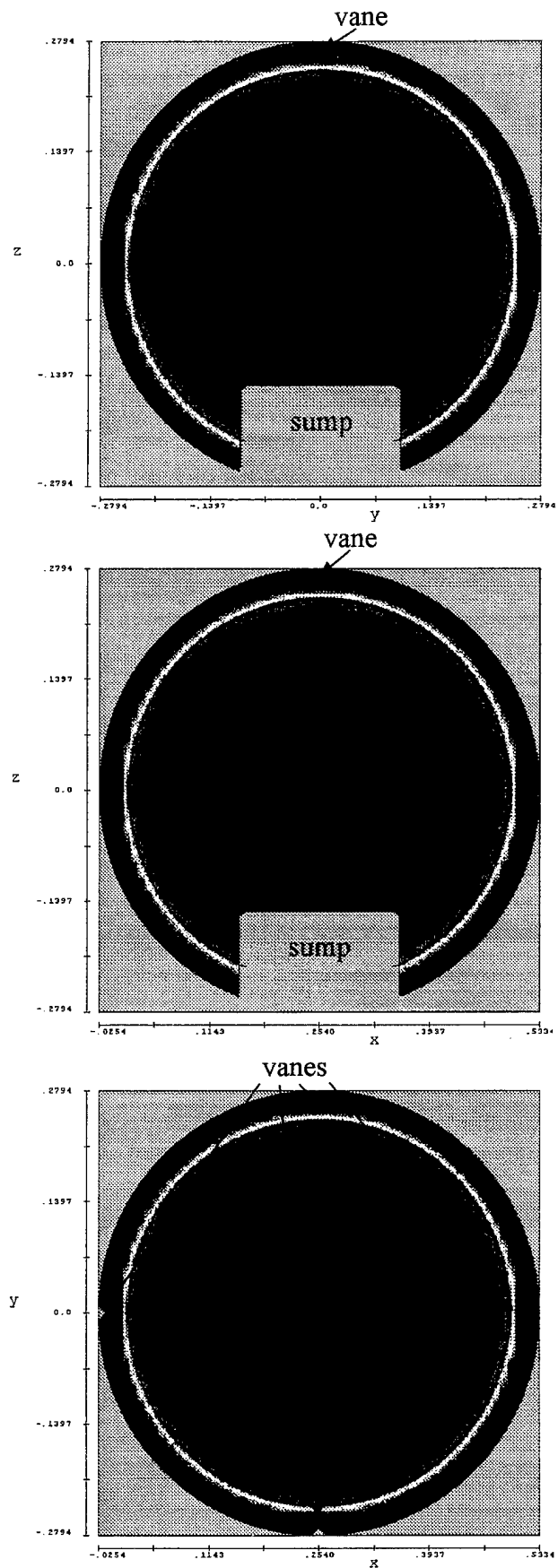
Figure 2: Initial fuel configuration for the low mass case (units in meters).

9
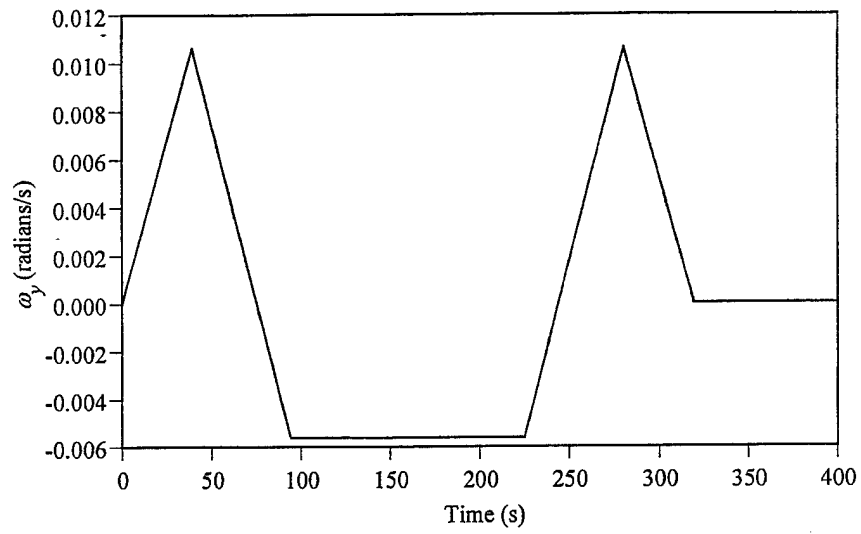
Figure 3: Specified angular velocity of the fuel tank about the origin
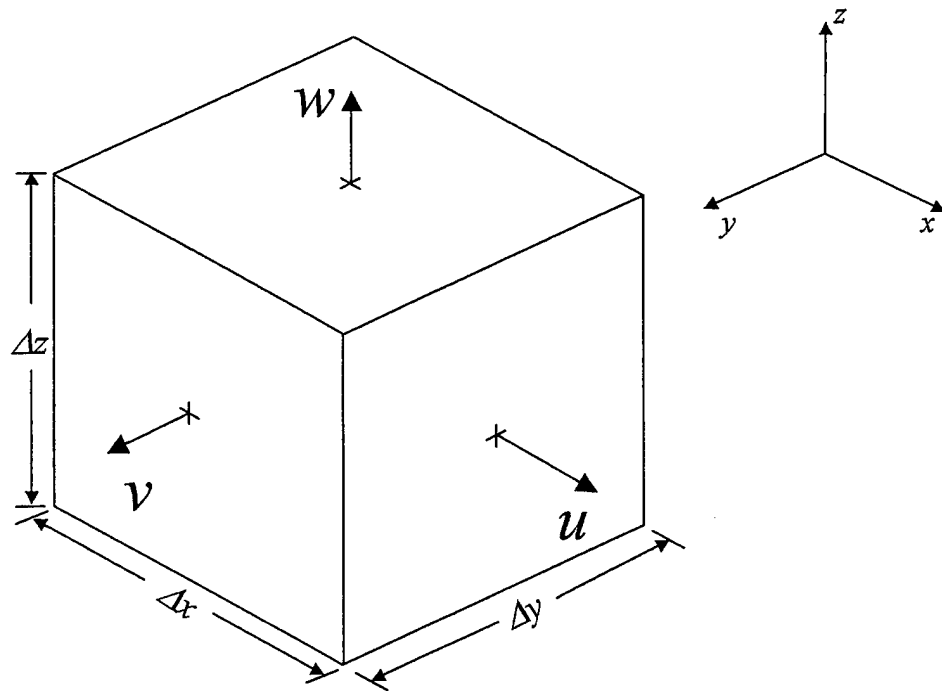
Figure 4: Computational cell

10
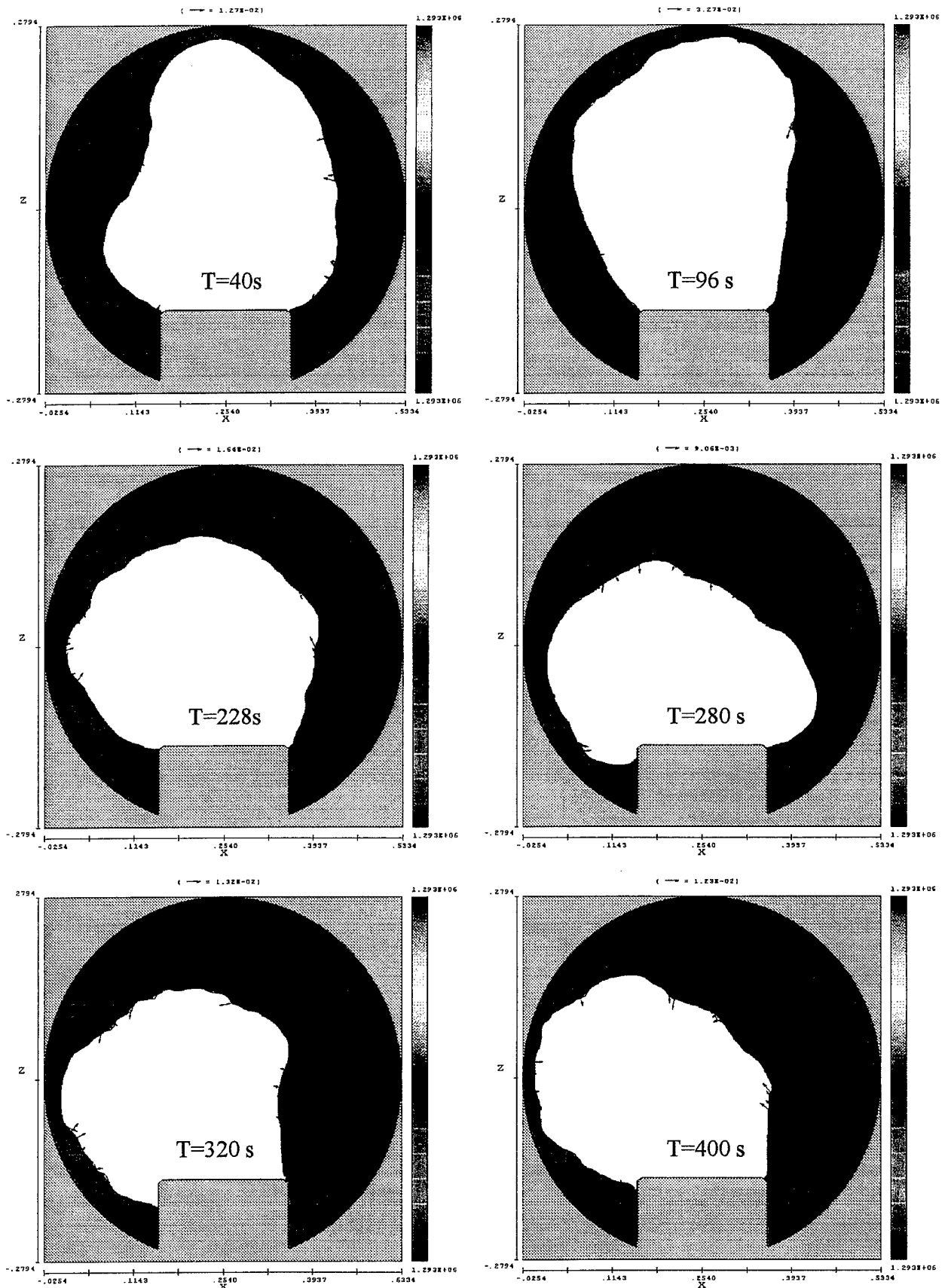
Figure 5: Pressure contours and velocity vectors for the high fuel mass case
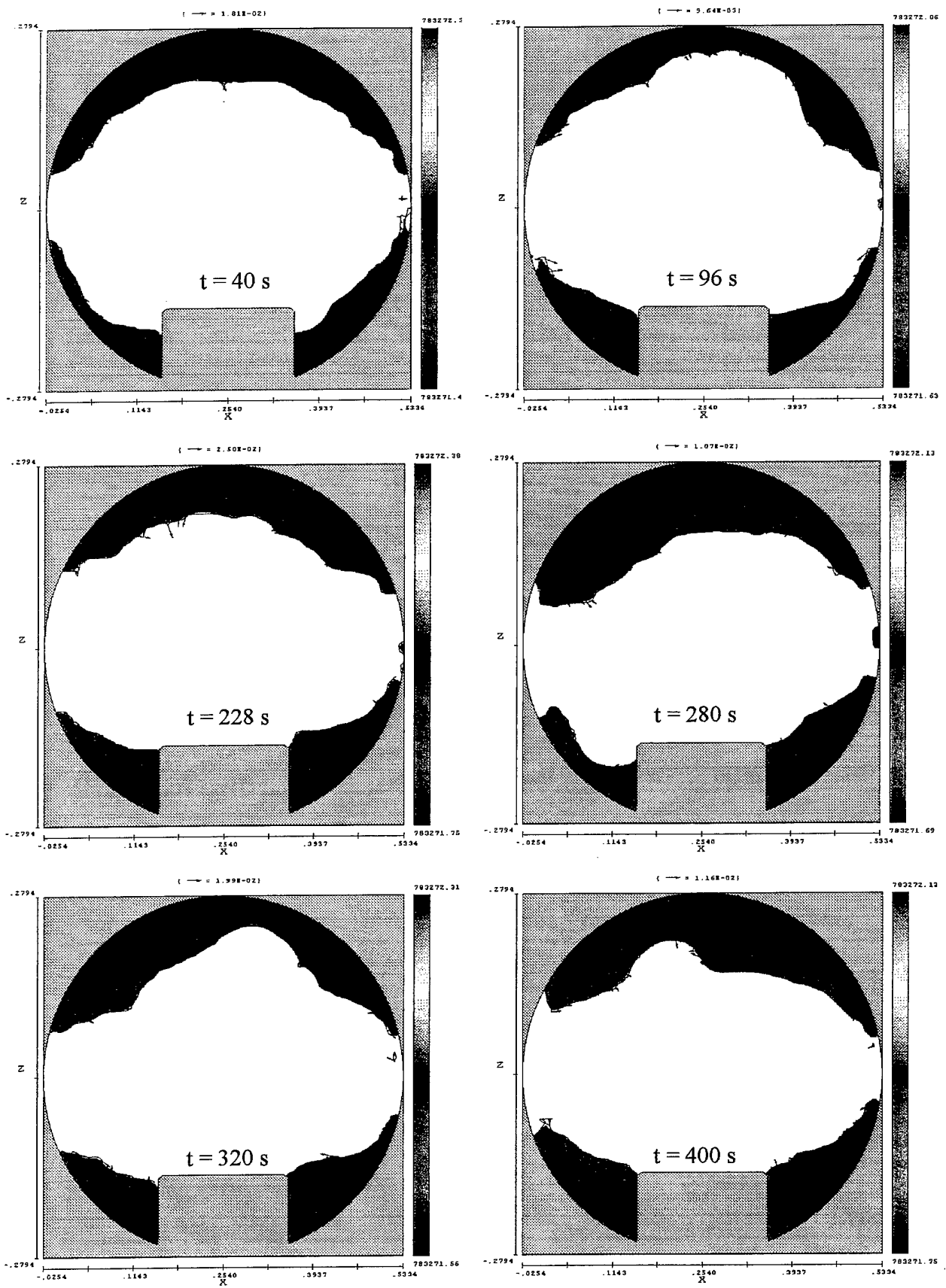
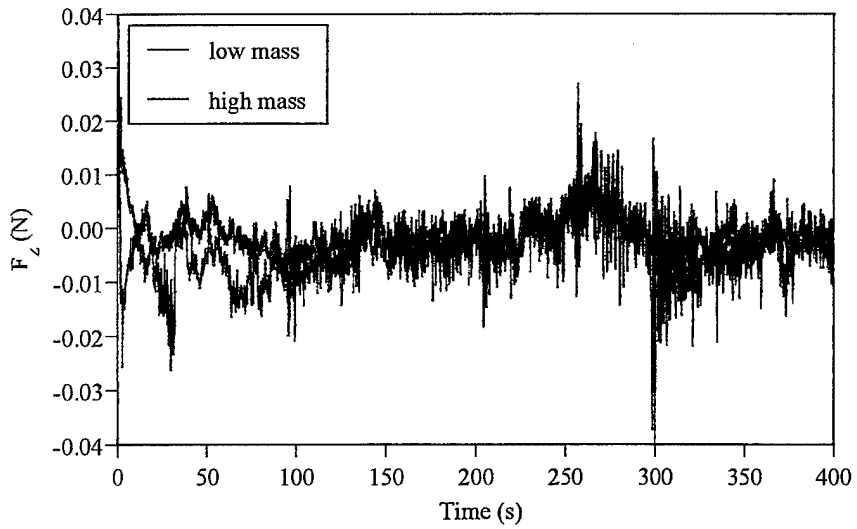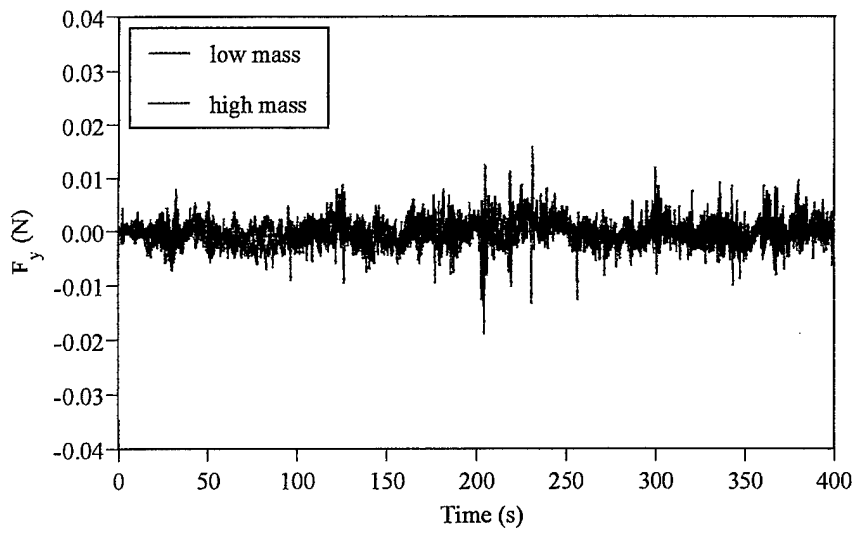Figure 6: Pressure contours (Pa) and velocity vectors (m/s) for the low mass case.
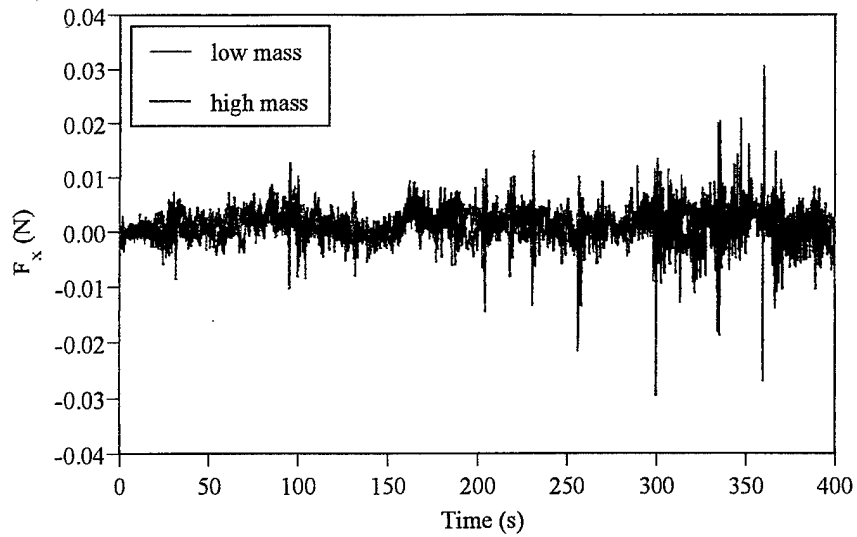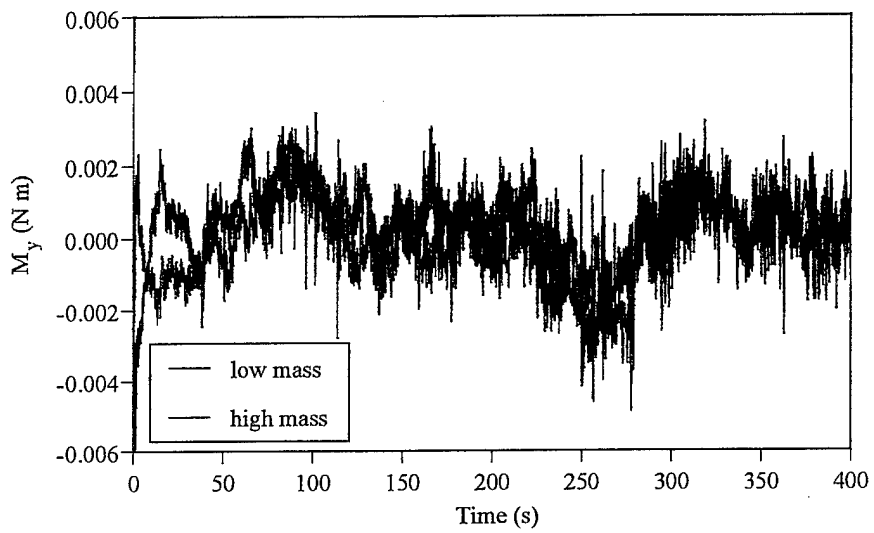
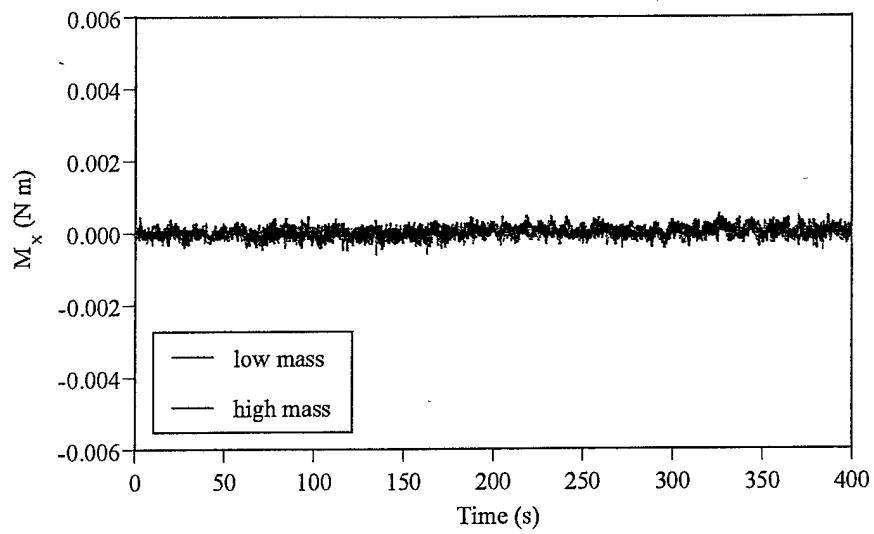Figure 7: Forces induced by fluid slosh acting on the tank
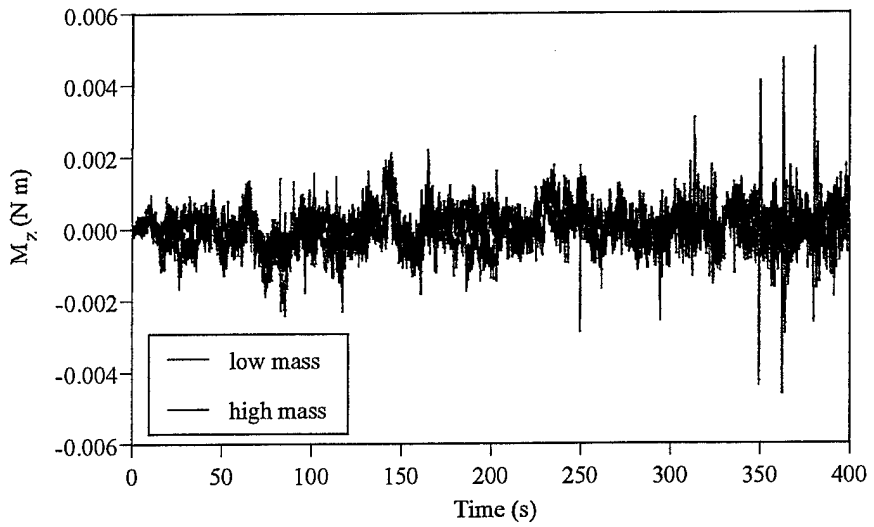
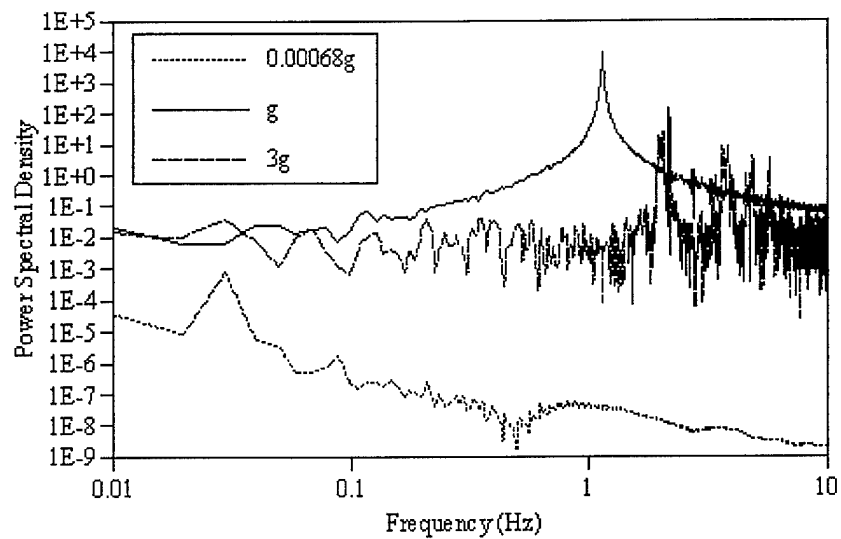Figure 8: Moments about the origin induced by fluid slosh

Figure 9: Power spectral density of the x slosh force.